Toward Targeted Retinal Drug Delivery with Wireless Magnetic Microrobots

Görkem Dogangil, Olgaç Ergeneman, Jake J. Abbott, Salvador Pané, Heike Hall,
Simon Muntwyler, and Bradley J. Nelson

Abstract— Retinal vein occlusion is an obstruction of blood flow due to clot formation in the retinal vasculature, and is among the most common causes of vision loss. Currently, the most promising therapy involves injection of t-PA directly into small and delicate retinal vessels. This procedure requires surgical skills at the limits of human performance. In this paper, targeted retinal drug delivery with wireless magnetic microrobots is proposed. We focus on four fundamental issues involved in the development of such a system: biocompatible coating of magnetic microrobots, diffusion-based drug delivery, characterization of forces needed to puncture retinal veins, and wireless magnetic force generation. We conclude that targeted drug delivery with magnetic microrobots is feasible from an engineering perspective, and the idea should now be explored for clinical efficacy.

I. Introduction

Retinal vein occlusion (RVO) is a common retinovascular disease caused by obstruction of blood flow due to clot formation. RVO is among the most common causes of vision loss around the world, with one study reporting a prevalence of 1.6% in adults aged 49 years or older [1]. To date, there is no effective clinical treatment for RVO. Various treatment methods for RVO have been proposed and attempted. However, due to excessive postoperative complications or inconclusive clinical trials of other methods, prolonged local intravenous thrombolysis (i.e., clot dissolution) with tissue plasminogen activator (t-PA) injection is the most promising treatment for RVO [2].

Retinal microsurgery requires precise manipulation that is constrained by the limits of human performance and perception [3], [4]. Retinal veins are small and delicate structures surrounded by fragile retinal tissue, and prolonged manual cannulation of retinal veins risks causing permanent physical damage to the retina. Robotic systems have been proposed to assist with retinal vein cannulation, utilizing robot-assisted surgical instruments that pass through a hole in the sclera, as in conventional vitreoretinal surgery [5], [6].

This paper presents the concept and feasibility study of an alternative approach to retinal therapy: the use of a wireless magnetic microrobot for targeted drug delivery (Fig. 1). The microrobot that is coated with clot-dissolving t-PA will be steered to the thrombus site as it is tracked visually through
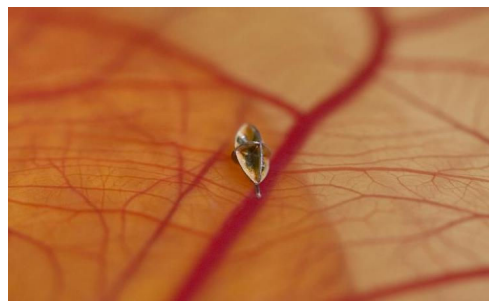
Fig. 1. Concept photo of a microrobot docked to a blood vessel for drug delivery. The assembled-MEMS microrobot shown is based on [7].

the pupil, and will insert its needle directly into the clot in the retinal veins. Diffusion of t-PA from the needle and the surface of the microrobot into the clotted region will start clot dissolution. There is strong evidence that t-PA in the preretinal area can diffuse into the retinal vasculature and break clots [8]. Since t-PA is an enzyme, and the clot dissolution reaction rate depends on enzyme reaction rate, long-term release of t-PA is thought to be more effective than bolus injections [9]. The proposed delivery mechanism provides an easy drug release without the need for a micropump, and an efficient therapy using small amounts of t-PA over prolonged periods. Moreover, a microrobot is potentially less invasive than other methods, and has the potential to be left in the eye for extended periods of time, even in an outpatient scenario.

This work focuses on the four fundamental issues in developing the microrobot as a targeted retinal drug delivery system. First, biocompatibility of the microrobot is achieved with titanium (Ti) coatings and demonstrated by *in vitro* toxicity tests. Second, diffusion-based drug delivery using Ti-coated microrobots is investigated experimentally. Third, the forces required for retinal vein cannulation are characterized experimentally. Finally, magnetic force that can be generated to achieve a puncture using the microrobot is analyzed.

II. Biocompatible Coating and Toxicity Tests

Electroplated microrobot pieces contain nickel (Ni). Ni and Ni compounds are declared to be non-biocompatible. Hence they are not used in medical devices. Ti and Ti alloys are used extensively in biomedical applications because of their excellent combination of biocompatibility, corrosion resistance, and structural properties [10]. In order to achieve biocompatibility without sacrificing the magnetic properties of Ni, microrobot pieces are coated with a thin layer of
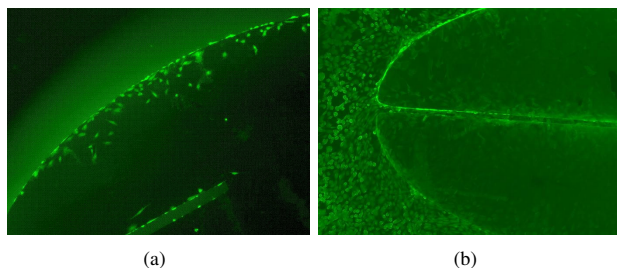
(a)   (b)

Fig. 2.   Cell proliferation on biocompatible microrobot pieces is clearly visible. Images taken on (a) 2nd day (b) 10th day show an increase in the number of live (fluorescent) cells. The slits on the pieces are $50\,\mu$m wide.

Fig. 3.   Fluorescence intensity vs. time for the release experiment.

Ti, forming a titanium dioxide layer once exposed to air. Coatings with thicknesses of $100\,$nm, $200\,$nm, $300\,$nm, and $500\,$nm have been made using a DC sputterer (Edwards Inc.). The coating quality, thickness, and uniformity are controlled using white-light interferometry and light microscopy.

Biocompatibility covers a broad spectrum of non-toxic and non-allergic properties, with various levels of biocompatibility associated with the purpose of a medical device. Bicompatibility tests involve toxicity tests, corrosion tests, and allergy tests. Due to the extensive literature on non-corrosive behavior and biocompatibility of Ti, corrosion and allergy tests were not conducted. However, to validate the quality of coatings against possible faults and crack formations, *in vitro* direct-contact cell-toxicity tests, in line with ISO 10993-5 8.3 standard, were performed on coated and uncoated microrobots, using NIH 3T3 fibroblast cells.

Approximately 100,000 cells per piece are placed in contact with coated and uncoated, sterilized microrobot pieces. Control sets are prepared without any pieces. Life-and-death-staining test is performed every 2 days for 10 days. Fluorescent staining solution is prepared with flurescein diacetate ($2.5\,\mu$g/mL), ethidium bromide ($10\,\mu$g/mL), and sterile phosphate buffered saline (PBS). Life and death of the stained cells are analyzed immediately with fluorescent microscopy, during which live cells emit bright green.

Results show that as thin as a 100-nm-thick Ti coating is sufficient to obtain biocompatibility. Fig. 2 shows the staining experiment for the 100-nm-thick-Ti-coated microrobot pieces on the 2th and 10th day after the start. Cell proliferation and growth are clearly visible, which points to the biocompatibility of Ti-coated microrobot pieces. Cell proliferation were also observed in the control group. No live cells were observed on the uncoated Ni pieces.

III. DRUG COATING AND RELEASE EXPERIMENTS

The developed microrobot constitutes a minimally invasive platform to deliver drugs to the retina using principles of diffusion. The clot dissolving drug used in RVO cases, t-PA, is an enzyme synthesized in human endothelial cells. Since it is an enzyme, it acts as a catalyst in the thrombolysis reaction, (i.e., it enters the reaction at a constant speed and is not consumed). The reaction rate of thrombolysis is based on the reaction rate of t-PA diffusion into the clot. With this in mind, a sm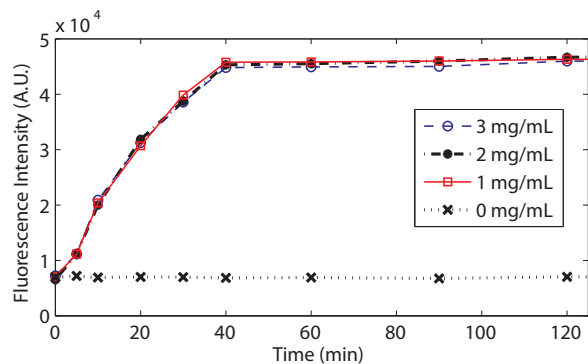all quantity of highly concentrated t-PA placed near the clot could be as effective as a bolus injection of t-PA in solution.

This section presents results of the preliminary drug release experiments using the untethered microrobot and discusses the feasibility of microrobotic drug delivery. A drug substitute is coated on microrobots, the release kinetics is characterized, and the amount of drug that can be coated in a single layer on a microrobot is quantified. The feasibility of drug release and drug release kinetics are demonstrated with this experiment.

A. Release Kinetics and Quantification

As a drug molecule substitute, bovine serum albumin (BSA) was chosen. BSA is a plasma protein that can be used as a blocking agent or added to diluents in numerous biochemical applications. BSA is used because of its stability, its inert nature in many biochemical reactions, its low cost, and its molecular size.

Four elliptical microrobot pieces of length $900\,\mu$m, width $450\,\mu$m, and thickness $50\,\mu$m are used. The pieces are first sterilized in ethanol and then washed with sterilized DI-water. Single microrobot pieces are placed in different wells of a 96-well culture plate. A sterilized BSA-solution of $3\,$mg/mL is prepared and labeled with Alexa-Fluor-546 (Molecular Probes) fluorescent marker. This solution is then mixed with sterilized PBS in order to create solutions with different concentrations of labeled-BSA molecules. Three of the microrobot pieces are dipped in BSA concentrations of $3\,$mg/mL, $2\,$mg/mL, $1\,$mg/mL, respectively, and one is dipped into a pure PBS solution, which contained no BSA, as a control set. The pieces are left in the solutions to allow the BSA to bind to the Ti. The surface-coating process is done for 12 hours at room temperature in a humidity chamber.

Coated microrobot pieces are taken from coating wells and placed in new wells filled with $200\,\mu$L PBS each. Following that, the florescence intensity is measured in set time intervals for three days using an automated spectrum analyzer (Tecan Infinite 200 Multiwell Plate Reader). In this way, the kinetics of diffusion-based drug delivery with surface-coated microrobots are obtained.

Fig. 3 quantifies the amount of time required to release the drug through diffusion, and it also gives qualitative

information about the kinetics of release. It is clear that the concentration of the coating solution does not affect the amount of drug bound to the Ti. This provides strong evidence that the amount of drug will be limited by the surface area of the microrobot.

Next, the amount of BSA released from a single piece is quantified. The release wells of the culture plates are analyzed in the multiwell plate reader for fluorescence and absorbance values. The BSA standard concentration curve is obtained by preparing a Bradford Assay with ten different known concentrations of BSA in 1:2 dilutions, and analyzing this assay for fluorescence and absorbance. The obtained standard curve is used to calibrate the multiwell plate reader. The fluorescence intensity in the release wells is measured and, using the calibration curve, the amount of BSA released is found to be $2.5 \pm 0.1 \, \mu$g per piece.

B. Multilayer Drug Coatings

In order to bind more proteins or drugs onto a microrobot of a given surface area, multilayer surface coatings or coatings embedded in different base matrices should be developed. Among others, hydrogels, agarose, starch microcapsulations, polymer matrices, liposomes, and biodegradable needles are widely used for making drug delivery matrices that can hold much more drug due to their material properties [11], [12], [13]. These materials can be used to encapsulate drug molecules as an outer coating, enabling multilayer coatings. These multilayer coatings can be used to coat multiple drug types on one microrobot, or used to fine tune delivery times or dosage. Alternatively, embedding drug molecules in a porous matrix facilitates slower diffusion and more drug loading capacity. Controlled release of drugs has been demonstrated using intelligent polymers that respond to stimuli such magnetic fields, ultrasound, temperature, and pH. These materials enable fine tuning of diffusive drug release.

IV. CHARACTERIZATION OF PUNCTURE FORCES

We propose a drug delivery method where the microrobot docks to a blood vessel to allow the drug to release over extended periods of time, as shown in Fig. 1. This will require a microneedle to puncture the blood vessel. The magnetic forces on microrobots in applied magnetic fields are well understood. However, the magnitude of forces needed to puncture retinal veins is not available in the literature. In this section, forces required for retinal vein punctures are measured and analyzed. In [3], retinal puncture forces together with the scleral interaction forces are measured. However, needle and blood-vessel size, which affect puncture forces, are not specified. In [4], a retinal pick equipped with strain gauges is used to manipulate the retina of porcine cadaver eyes, and the range of forces acquired during a typical procedure is reported. However, the force of an individual retinal vein puncture is not provided. Conducting *in vivo* experiments on animal eyes is difficult with a high risk of tissue damage, and postmortem experiments may
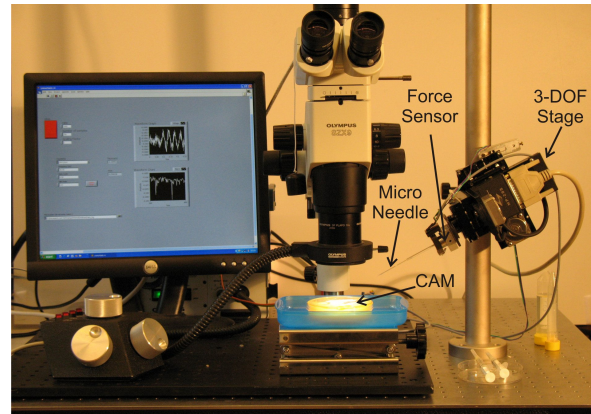
(a)
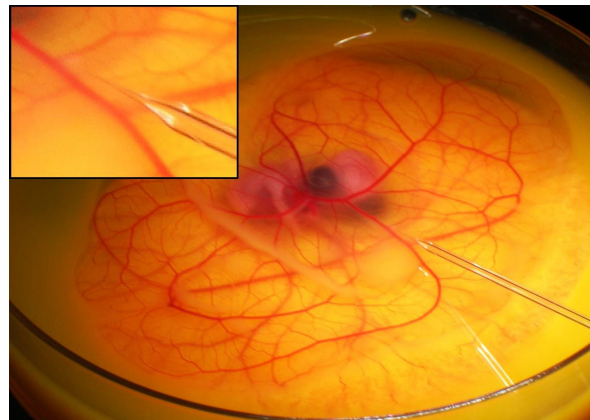
(b)

Fig. 4.   (a) Experimental setup. (b) Close-up view of chicken CAM and the microneedle in the setup during an experiment.

provide inaccurate results due to rapid changes in tissue properties of vessels after death.

In this section, experimental data is collected from the vasculature of chorioallantoic membranes (CAM) of developing chicken embryos. The CAM of the developing chicken embryo has been used by ophthalmologists as a model system for studying photodynamic therapy and ocular angiogenesis. Recently, it was reported that the CAM of a twelve-day-old chicken embryo is a valid test bed for studies on human retinal vessel puncture [14]. The CAM's anatomical features and physiologic and histologic responses to manipulation and injury make it an effective living model of the retina and its vasculature. The vasculature of a twelve-day-old CAM and a human retina have roughly the same diameter and wall thickness (i.e., vessels with 100–300 μm outer diameter).

A. Experimental Setup

The custom experimental setup shown in Fig. 4 is used to measure vessel puncture forces. The setup consists of a microscope (Olympus SZX9), a digital camera (Basler A602fc) delivering images and real-time video to a PC, several light sources, a capacitive force sensor (Neonics Inc.)

with an attached microneedle, mounted on a 3-DOF Cartesian micromanipulator (Sutter Instruments, MP-285), and a hot pack to keep the embryo warm during the experiments. Measured voltages are sampled at 1 kHz and lowpass filtered in Labview 8.1 to eliminate noise.

The force sensor is calibrated using a microscale (Acculab VI-1mg) before each experiment. The estimated sensor gain has a 95% confidence interval of $\pm 2.9\%$. During the experiments, as the sensor is used in a tilted position, the gain of the sensor changes slightly due to the weight of the attached microneedle. To account for this effect on non-vertical measurements, a tilted sensor with an attached pipette was calibrated using a custom MEMS force sensor [15], whose gain does not change with angle owing to its design. The estimated sensor gain at $63°$ from vertical, which is the angle at which the experiments are conducted, has a 95% confidence interval of $\pm 11.5\%$. The sensor is recalibrated before starting each experiment in order to account for the change of needles.

Six sets of microneedles with different outer diameters (OD) were prepared for the experiments. They were pulled out of 1 mm OD boron-silicate glass pipettes in a repeatable way using a pipette puller (DMZ Universal Puller, Zeitz Inst., Germany). The needle ODs were measured with a microscope, and the average values of the six sets are found in μm as: 3.3, 6.7, 43, 59, 76, 90. The measurement errors were $\pm 0.5\,\mu$m and $\pm 2\,\mu$m for ODs smaller and larger than $10\,\mu$m, respectively.

B. Experimental Procedure

Twelve-day-old embryos are used in the experiments. Fertilized chicken eggs are bred in incubators at 55% relative humidity and 37°C ambient temperature. At the end of the third day of incubation, the eggs are carefully cracked and the contents are transferred into a Petri dish, which is a different method for CAM preparation than used in previous studies that prepared the CAM intact in the egg shell [5], [14]. The embryos are incubated for another nine days until the experiment in the Petri dish, which enables easy access for the experiments.

During an experiment, a target blood vessel is selected, and vessel diameter measurements are made in the image obtained from the microscope, with an error of $\pm 2\,\mu$m. The micromanipulator, which is holding the force sensor with the attached microneedle, is advanced along the direction of the microneedle's axis, and the puncture is done under direct observation through the microscope as force measurements are taken. The experiments are also captured on video. During the experiments, the actual puncture and blood flow is easily observed with the microscope. Sterile neutral PBS of pH 7.1 is used to keep the CAM surface moist and soft. This also improves visualization through the microscope.

Puncture of a CAM vessel is difficult due to the elasticity of the CAM membrane. The deformation is an artifact of using a CAM model, and is not present in actual retinal vein puncture. To make puncture easier, the membrane in proximity to the target vessel is fixed by a rigid clamp,
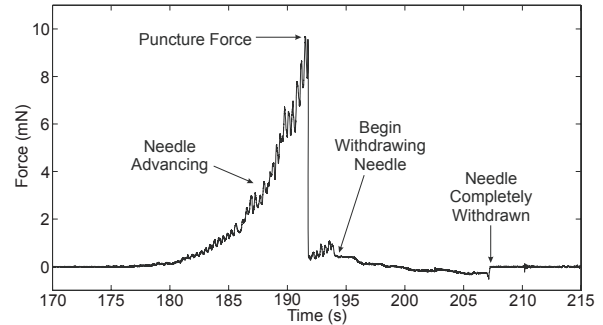

Fig. 5. Force vs. time data during the puncture of a 280-μm-OD vessel with a 76-μm-OD microneedle. The puncture event is clearly visible.

mitigating membrane deformation. Moreover, due to the elasticity of the blood vessels themselves, pushing the needle with an angle of incidence of $0°$ (i.e., the angle between the axis of the needle and vertical) pushes the entire vessel rather than cannulating it, and when it finally punctures, the bounce is usually high enough to puncture the far wall of the vessel as well, resulting in a ruptured vessel and excessive bleeding. Due to the setup limitations, such as the height of the petri-dish wall and proximity of the microscope lens, the most effective angle of incidence was found to be $63°$ for luminal punctures. In this configuration, single-wall punctures are observed, and excessive force drives the needle into the vein lumen rather than causing a second puncture.

While the experiments are observed through the microscope and the live video feed, the instant of puncture is first verified visually by the operator. Success or failure of a cannulation is determined by whether the post-puncture bleeding is only on top of the CAM or also under it. The blood vessels are embedded in the CAM [14] in such a way that they do not bleed under it unless the vessel is also punctured on the far side. At the instant of puncture, the real-time force plot shows a sudden drop due to the needle breaking through to the lumen of the blood vessel. Fig. 5 shows the force plot of a typical puncture experiment.

C. Results and Discussion

Figure 6 shows the results of the vessel puncture experiments. The experiments were conducted with 32 embryos resulting in a total of 241 successful punctures. For every needle diameter and vessel diameter, three consecutive cannulations are made for statistical purposes. As seen on the plots, there is variance in the force data due to effects that are not accounted for, such as anatomical variance between individual vessels and embryos, the state of the embryo (e.g., blood pressure, temperature), non-Hookean behavior of the vessel walls, errors in measured microneedle diameter, and error in the angle of incidence of the microneedle with respect to the blood vessel. Despite the variance, the data exhibit clear trends. We observed an approximately quadratic trend in blood-vessel diameter and an approximately linear trend in microneedle diameter.

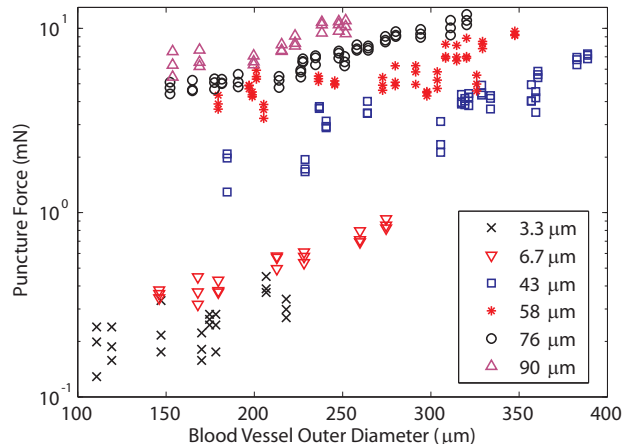The experiments are performed with blunt-tip needles, so

Fig. 6. Experimental data of puncture force vs. vessel diameter for different microneedles ODs.

the forces shown in Fig. 6 should be taken as upper bounds for required puncture forces. It is known that beveling the needle's tip will reduce the puncture forces [16], [17].

In [4], it is shown that 88% of all tool/tissue interaction forces during vitreoretinal surgery are below 12.5 mN, which corresponds well with our results shown in Fig. 6. In [3], higher puncture forces with larger variance than our results are reported. However, the reported forces include scleral interaction forces, and the force sensor is mounted on a handheld device.

V. Generating Magnetic Force

Wireless control of the microrobots discussed in this paper is achieved using magnetic fields. Calculating magnetic torque and force on permanent-magnetic bodies is straightforward, requiring knowledge only of the remanence magnetization and volume of material. Simple models for magnetic torque and force on axially symmetric [18] and assembled-MEMS [19] soft-magnetic bodies have been developed; these models require knowledge of body geometry and saturation magnetization of the material. In this paper, we are concerned with the amount of force that can be developed wirelessly for the purpose of puncturing retinal veins.

The force on a magnetic dipole is given by

$$\mathbf{F} = \mu_0 v \left(\mathbf{M} \cdot \nabla\right) \mathbf{H} = v \left(\mathbf{M} \cdot \nabla\right) \mathbf{B} \qquad (1)$$

in N, where $\mu_0 = 4\pi \times 10^{-7}$ T·m/A is the permeability of free space, ∇ is the gradient operator, v is the volume of magnetic material in m^3, $\mathbf{M}$ is the magnetization in A/m, and $\mathbf{H}$ and $\mathbf{B}$ represent the applied magnetic field described in A/m and T, respectively. In permanent magnets, $\mathbf{M}$ is effectively constant, but it is a function of the applied field in soft-magnetic materials. Simply stated, the magnetic force in any direction x is calculated as the dot product of the derivative of the field, $d\mathbf{B}/dx$, and the magnetic moment $v\mathbf{M}$.

Let us consider a microrobot assembled from two thin elliptical pieces, as shown in the inset of Fig. 7. The volume

of this microrobot is given by $v = 2\pi abt - 2at^2$. We measured the force on such assembled microrobots made of Ni and CoNi using the magnetic measurement system described in [20], and the results are shown in Fig. 7. The system uses a $40\,\text{mm} \times 40\,\text{mm} \times 20\,\text{mm}$ NdFeB magnet with the north and south poles on the largest faces, and a field value of 0.41 T measured in the center of the north pole face. In addition to the measured data, we simulated a microrobot made of permanent-magnetic material with a remanence magnetization of 4×10^5 A/m, which is a value that can currently be achieved using microfabrication techniques [21].

In Fig. 7 we see that magnetic force drops off rapidly with increasing distance between the microrobot and the magnet. Increasing the saturation magnetization of a soft-magnetic material (compare CoNi and Ni) can lead to increases in force in a high-field region. Even relatively poor soft-magnetic materials (Ni) match good permanent magnets in a high-field region since the saturation magnetization values for soft-magnetic materials are typically higher than the remanence magnetization values of permanent magnets. However, as field strength is reduced, and the soft-magnetic microrobots are no longer saturated, they begin to provide similar force, and each provides less than that of the permanent-magnetic material. This is due to the magnetization of the soft-magnetic material, which is a function of the applied field, dropping below the remanence of the permanent-magnetic material.

Let us consider a microrobot with dimensions $a = 1000\,\mu\text{m}$, $b = 500\,\mu\text{m}$, and $t = 100\,\mu\text{m}$, and a volume of $v = 3 \times 10^{-10}\,\text{m}^3$; this microrobot could be electroplated and assembled, and fit through a 1-mm incision. If we consider the microrobot at a position 70 mm away from the surface of the magnet, soft- and permanent-magnet materials provide approximately the same force of 0.05 mN. For a length comparison, the diameter of the human eye is 25 mm, so this places the surface of the magnet almost three eye diameters away from the microrobot. If we move the microrobot only about 10 mm closer to the magnet, we gain an order of magnitude in our magnetic force, bringing it beyond the level needed for puncturing retinal veins with a blunt-tip needle of a few micrometers in size. As mentioned previously, beveling the needle's tip would reduce the required force even further. The magnet used in the experiment was chosen somewhat arbitrarily; other magnet shapes and sizes can be chosen to project the magnetic field at greater distances.

Under the above considerations, it seems feasible that enough magnetic force can be developed by pulling with magnetic field gradients to puncture retinal veins, provided that the microneedle is made small enough and sharp enough. These demands are attainable with current microfabrication technology. Puncture also requires an intelligent design of the magnetic-field generation system, which will use the superimposed fields of multiple permanent magnets or electromagnets, increasing the ability to generate strong fields at a distance. The choice of soft- or permanent-magnetic material for the microrobot will ultimately depend on the design of the magnetic-field generation system. In addition, it
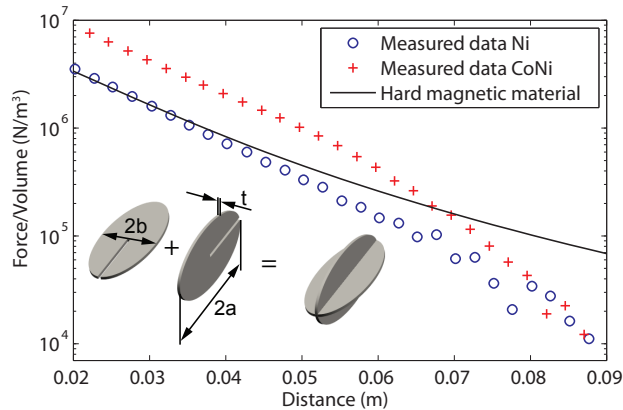
Fig. 7. Experimental data of normalized force vs. distance of the microrobot from the magnet's surface. The magnet is described in [20]. A simulation of permanent-magnetic material with a remanence of 4×10^5 A/m is also shown. (Inset) Definition of dimensions of the assembled microrobots used.

was recently shown that microrobots that swim using helical propellers that mimic bacterial flagella theoretically have the potential to develop higher forces than obtained with gradient-based force generation at these small scales [22]. This provides another option for retinal drug delivery.

VI. CONCLUSION AND FUTURE WORK

In this paper, fundamental aspects of the development of a novel system for minimally invasive targeted retinal drug delivery using wireless magnetic microrobots was presented. Biocompatibility of the microrobots was achieved by sputtering thin layers of Ti, and verified using a standardized cell-toxicity test. This sputtering method can be used to create a uniform coating of Ti even on complicated geometries. Initial experiments on diffusion-based drug delivery using coated microrobots were conducted, providing knowledge of quantity and kinetics of drug release. Future work will consider advanced coating techniques to load more drug onto microrobots, and to control the drug delivery kinetics. Retinal cannulation forces were characterized by measurements on the vasculature of chorioallantoic membranes of live chicken embryos, and the relationship between puncture force and blood-vessel and needle diameters was investigated. Magnetic force generation was analyzed by comparing required puncture forces to measured magnetic forces and previously developed models. We find that puncturing retinal veins using magnetic microrobots will require small and sharp microneedles and a well-designed magnetic-field generation system. We conclude that targeted drug delivery with magnetic microrobots is feasible from an engineering perspective, and the idea should now be explored for clinical efficacy.

ACKNOWLEDGMENT

REFERENCES

[1] W. M. Tang and D. P. Han, "A study of surgical approaches to retinal vascular occlusions," *Arch. Ophthalmol.*, vol. 118, pp. 138–143, 2000.

[2] H. Shahid, P. Hossain, and W. M. Amoaku, "The management of retinal vein occlusion: Is interventional ophthalmology the way forward?" *British J. Ophthalmol.*, vol. 90, pp. 627–639, 2006.

[3] A. D. Jagtap and C. N. Riviere, "Applied force during vitreoretinal microsurgery with handheld instruments," in *Proc. IEEE Int. Conf. Eng. Med. Biol. Soc.*, 2004, pp. 2771–2773.

[4] P. K. Gupta, P. S. Jensen, and E. de Juan, Jr., "Surgical forces and tactile perception during retinal microsurgery," in *Proc. Int. Conf. Med. Image Comput. and Comput.-Assisted Intervention*, 1999, pp. 1218–1225.

[5] B. Mitchell, J. Koo, I. Iordachita, P. Kazanzides, A. Kapoor, J. Handa, G. Hager, and R. Taylor, "Development and application of a new steady-hand manipulator for retinal surgery," in *Proc. IEEE Int. Conf. Robot. Autom.*, 2007, pp. 623–629.

[6] C. N. Riviere, W. T. Ang, and P. K. Khosla, "Toward active tremor canceling in handheld microsurgical instruments," *IEEE Trans. Robot. Autom.*, vol. 19, no. 5, pp. 793–800, 2003.

[7] K. B. Yesin, K. Vollmers, and B. J. Nelson, "Modeling and control of untethered biomicrorobots in a fluidic environment using electromagnetic fields," *Int. J. Robot. Res.*, vol. 25, no. 5–6, pp. 527–536, 2006.

[8] N. G. Ghazi, B. N. Noureddine, R. S. Haddad, F. A. Jurdi, and Z. F. Bashshur, "Intravitreal tissue plasminogen activator in the management of central retinal vein occlusion," *Retina*, vol. 23, 2003.

[9] M. K. Tameesh *et al.*, "Retinal vein cannulation with prolonged infusion of tissue plasminogen activator (t-PA) for the treatment of experimental retinal vein occlusion in dogs," *Am. J. Ophthalmol.*, vol. 138, no. 5, pp. 829–839, 2004.

[10] B. D. Ratner, A. S. Hoffman, F. J. Schoen, and J. E. Lemons, Eds., *Biomaterials Science: An Introduction to Materials in Medicine*, 2nd ed. Elsevier Academic Press, 2004.

[11] X. Cao, S. Lai, and L. J. Lee, "Design of a self-regulated drug delivery device," *Biomedical Microdevices*, vol. 3, no. 2, pp. 109–118, 2001.

[12] A. S. Lubbe, C. Alexiou, and C. Bergemann, "Clinical applications of magnetic drug targeting," *J. Surgical Research*, vol. 95, pp. 200–206, 2001.

[13] J.-H. Park, M. G. Allen, and M. R. Prausnitz, "Polymer microneedles for controlled-release drug delivery," *Pharm. Research*, vol. 23, no. 5, pp. 1008–1018, 2006.

[14] T. Leng, J. M. Miller, K. V. Bilbao, D. V. Palanker, P. Huie, and M. S. Blumenkranz, "The chick chorioallantoic membrane as a model tissue for surgical retinal research and simulation," *Retina*, vol. 24, no. 3, pp. 427–434, 2004.

[15] Y. Sun, B. J. Nelson, D. P. Potasek, and E. Enikov, "A bulk microfabricated mulit-axis capacitive cellular force sensor using transverse comb drives," *J. Micromechanics Microeng.*, vol. 12, no. 6, pp. 832–840, 2002.

[16] S. P. Davis, B. J. Landis, Z. H. Adams, M. G. Allen, and M. R. Prausnitz, "Insertion of microneedles into skin: Measurement and prediction of insertion force and needle fracture force," *J. Biomechanics*, vol. 37, pp. 1155–1163, 2004.

[17] N. Abolhassani, R. Patel, and M. Moallem, "Needle insertion into soft tissue: A survey," *Medical Engineering and Physics*, vol. 29, pp. 413–431, 2007.

[18] J. J. Abbott, O. Ergeneman, M. P. Kummer, A. M. Hirt, and B. J. Nelson, "Modeling magnetic torque and force for controlled manipulation of soft-magnetic bodies," *IEEE Trans. Robot.*, vol. 23, no. 6, pp. 1247–1252, 2007.

[19] Z. Nagy, O. Ergeneman, J. J. Abbott, M. Hutter, A. M. Hirt, and B. J. Nelson, "Modeling assembled-MEMS microrobots for wireless magnetic control," in *Proc. IEEE Int. Conf. Robot. Autom.*, 2008.

[20] M. P. Kummer, J. J. Abbott, K. Vollmers, and B. J. Nelson, "Measuring the magnetic and hydrodynamic properties of assembled-MEMS microrobots," in *Proc. IEEE Int. Conf. Robot. Autom.*, 2007, pp. 1122–1127.

[21] L. Vieux-Rochaz, C. Dieppedale, B. Desloges, D. Gamet, C. Barragatti, H. Rostaing, and J. Meunier-Carus, "Electrodeposition of hard magnetic CoPtP material and integration into magnetic MEMS," *J. Micromech. Microeng.*, vol. 16, pp. 219–224, 2006.

[22] J. J. Abbott, K. E. Peyer, L. X. Dong, and B. J. Nelson, "How should microrobots swim?" in *Int. Symp. Robotics Research*, 2007.